Down-regulation of vinculin upon MK886-induced apoptosis in LN18 glioblastoma cells

A. M. MAGRO[1*], A. D. MAGRO[1], C. CUNNINGHAM[2], M. R. MILLER[3]

[1]Department of Biology, Fairmont State University, Fairmont, WV 26554, e-mail: amagro@fairmontstate.edu; [2]Departments of Microbiology, Immunology and Cell Biology and [3]Biochemistry and Molecular Pharmacology, Robert C. Byrd Health Sciences Center, West Virginia University, Morgantown, WV 26508

Received March 22, 2007

Glioblastomas are a type of malignant brain tumor and are among the most difficult cancers to treat. One strategy to treat aggressive cancers is the use of drugs that target multiple signaling pathways. MK886 is a drug known to inhibit both 5-lipoxygenase-activating-protein (FLAP) and peroxisome proliferator activated receptor-α (PPAR-α). The objectives of this study were to investigate the ability of MK886 to induce apoptotic cell death in LN18 glioblastoma cells and to characterize the cell death mechanisms. MK886 induced massive apoptotic LN18 cell death that was manifested by the release of nucleosomes, annexinV binding to phosphatidylserine in the absence of nuclear staining, and changes in the fluorescent intensity of Mito Tracker Deep Red 633 indicating changes in mitochondrial oxidative function and mass. The alteration of the mitochondrial function implied that MK886 induced apoptosis in LN18 cells via a mitochondrial pathway. The broad caspases inhibitor ZVAD-FMK inhibited MK886-induced nucleosome release, but not annexinV binding or MK886-altered mitochondrial function. Real time RT-PCR demonstrated that LN18 cells expressed significant levels of FLAP and PPAR-α mRNAs. A low level of arachidonate 5-lipoxygenase (ALOX-5) mRNA was detected, but little, if any, arachidonate 12-lipoxygenase (ALOX-12) mRNA was present. In addition, MK886-induced apoptosis in LN18 cells was accompanied by a decrease in the protein and mRNA levels of vinculin, but not other focal adhesion proteins. In summary, the data presented here indicate that disruption of the actin-vinculin-cell-cytoskeleton matrix of the LN18 glioblastoma is a component of the MK886 induced apoptosis. In addition, MK886 treated LN18 cells could provide one model in which to investigate drugs that target lipoxygenase and PPAR-α pathways in the chemotherapeutic treatment of glioblastomas.

Key Words: Glioblastoma; Apoptosis; PPAR-α; FLAP; 5-Lipoxygenase; MK886

Chemotherapeutic regimens for glioblastomas and other high grade gliomas have fallen short of providing effective treatment. Clinical studies comparing chemotherapeutic agents have indicated increased tumor shrinkage and a very slight increase in median survival times, but no evidence for an increase in survival rates [1]. More recent clinical studies using chemotherapeutic regimens either in combination with radiation therapy [2] or in combination with gene silencing regimens [3] are slightly more effective in increasing median survival times, but again have had limited success in increasing the overall survival rate in patients being treated for primary or recurrent glioblastoma. Clinical trials have produced no clear direction about which chemotherapeutic agents, or approaches, could improve survival rates in the treatment of glioblastomas.

One chemotherapeutic approach to treat difficult cancers is to develop drugs that target multiple pathways. 5-Lipoxygenase activating protein (FLAP) binds arachidonate and facilitates its interaction with arachidonate 5-lipoxygenase (ALOX-5), forming a complex in association with the nuclear envelope to promote leukotriene synthesis. MK886 (3-[1-(4-chlorobenzyl)-3-t-butyl-thio-5-isopropylindol-2-yl]-2, 2-dimethylpropanoic acid) is a hydrophobic indole that is known to bind FLAP. It is well established that MK886 inhibits the action of FLAP and blocks the formation of leukotrienes generated by the ALOX-5 pathway [4–6]. Inhibition of the lipoxygenase pathway has been shown to induce apoptosis in a variety of cancer cells [7–10] and in combination with COX-2 blockers can inhibit angiogenesis [11, 12].

*Corresponding author

However, MK886 induces apoptosis in cells that do not express FLAP [13], indicating an additional or alternative pathway(s) by which MK886 can induce apoptosis. Peroxisome proliferator activated receptors (PPAR) are a family of nuclear receptors that have been shown to be activated by leukotriene B4 and the eicosanoid 8(S)-hydroxyeicosatetraenoic acid [14, 15] as well as a number of fibrate drugs and fatty acids [16, 17]. In cells other than glioblastomas, Kehrer et al. [18] demonstrated that MK886 is a potent, noncompetitive inhibitor of peroxisome proliferator activated receptor alpha (PPAR-α) and therefore identified PPAR-α as a potential target of the drug MK886. While the extent to which PPAR-α is directly involved in MK886-induced apoptosis is not yet fully understood [18], MK886 clearly can target multiple signaling pathways.

The present investigation was initiated to determine the sensitivity of LN18 glioblastoma cells to MK886. An additional aim was to determine if FLAP and PPAR-α are expressed in LN18 cells and to use MK886 as a model compound to begin to characterize the apoptotic effects that occur by the simultaneous inhibition of both PPAR-α and FLAP dependent pathways in the LN18 glioblastoma cell line.

Materials and methods

Cell Type and Culture Conditions. The LN18 cell line (the ATCC, CRL-2610) was established in 1976 from a patient with a right temporal lobe glioma. The cells are poorly differentiated, adherent, and grow well in culture [19]. LN18 cells were maintained in Dulbecco's Modified Eagle Medium, free of phenol red and supplemented with the dipeptide L-alanyl-L-glutamine (2 mM), non-essential amino acids, pyruvate (100µg/ml), penicillin (100 units/ml), streptomycin (100µg/ml), amphotericin B (0.25µg/ml), HEPES (2 mM), and fetal bovine serum (10%), at 37°C in an atmosphere of 5% CO_2. Cells were subcultured by trypsinization (0.25% trypsin, EDTA). Medium and all cell culture reagents were purchased from Invitrogen. MK886 (Sigma-Aldrich) was dissolved in DMSO and diluted to the indicated concentrations in the Dulbecco's culture medium. All plasticware (Costar) used for tissue culture and other experimentation were purchased from Fisher.

Apoptosis Assayed by Fluorescent Microscopy, ELISA, AnnexinV Binding and Changes in Mitochondrial Potential. For examination by fluorescent microscopy, cells were plated onto 8 chambered glass slides (Lab Tech II) at $2x10^4$ cells/chamber. Following adherence and treatment the cells were fixed with 0.1% paraformaldehyde-PBS for 15min at room temperature and then permeabilized with 0.5% Triton X-PBS for 15min at room temperature. For actin and vinculin staining cells were incubated with Alexa Fluor phalloidin 488 (200 units/ml Rx, Molecular Probes) and anti-vinculin (10µg/µl Rx, Upstate, Clone V284) for 45min in the dark at room temperature. Following washing with PBS, cells were incubated with goat anti-mouse-IgG conjugated to Cy3 (15µg/µl Rx, Jackson ImmunoResearch) for 30 min in the dark at room temperature. Cells were then washed with PBS and the monolayer was examined by fluorescent microscopy (Nikon Diaphot).

Soluble DNA-histone complexes in the cytosol were detected in 96 well plates by an ELISA technique. LN18 cells were plated in 96 well microtiter plates ($1x10^4$ cells/well). Following adherence, the cells were treated with the indicated concentrations of MK886 for 10h or 15h. Cells were carefully rinsed and permeabilized by adding lysis buffer. After centrifugation, supernatants of the permeabilized cells were transferred to strepavidin-coated 96 well microtiter plates and tested for DNA-histone complexes by ELISA using anti-histone-biotin-antibody followed by peroxidase conjugated anti-DNA using 2,2'-azino-bis (3-ethylbenzthiazoline-6-sulfonic acid) as substrate (Roche Cell Death Detection ELISA kit). The development of product was measured in a Dynatech Microplate Reader at 405nm.

Apoptosis was demonstrated by established tests, including morphological changes, the release of histone-associated-DNA-fragments from the nucleus into the cytoplasm, annexinV binding to membrane-exposed phosphatidylserine and changes in mitochondrial function and mass. AnnexinV-FITC binding to phosphatidylserine in the absence of nuclear staining by propidium iodide (Roche, AnnexinV-FLOUS kit) was determined by flow cytometry. For those experiments in which the cells were fixed nuclear staining was detected by the irreversible nuclear binding dye 7-Amino-actinomycinD (7-AAD). Changes in the mitochondrial mass and oxidative function were detected by changes in fluorescent intensity of the mitochondrial membrane binding dye Mito Tracker Deep Red 633 (Molecular Probes). Following labeling, cells were analyzed with Becton-Dickinson FACSCalibur (San Jose, CA) using CellQuest Pro software. To determine the extent to which apoptotic changes were caspases dependent, some experiments were performed in the presence of 50µM of the caspases inhibitor ZVAD-FMK.

Real Time RT-PCR. Total cellular RNA was isolated using TRIZOL Reagent, following manufacturer's instructions (Life Technologies). Reverse transcriptase generated c-DNA(s) were obtained using random hexamers with the high capacity archive kit (Applied Biosystems) from RNA concentrations of 6.25ng/µl. The c-DNA(s) were allowed to form for 2h at 37°C. Negative controls were generated by omitting the reverse transcriptase in the cDNA-generating step. For the PCR step, the primers and Taq-Man fluorescent probes were purchased from Applied Biosystems. The primers were designed to span an intron to avoid amplification of any contaminating DNA. Real time PCR was performed using the Applied Biosystems Gene Amp 5700 system with the Taq-Man Universal PCR Master Mix. Relative mRNA levels were measured using the cycles to threshold (Ct) method, defined as the cycle number that first gives detection of the PCR amplicons above a fixed threshold baseline set within the log phase of the plot of fluorescence versus cycle number. There were 4 replicates

for each sample. The amplicons were generated over 40 cycles where each cycle consisted of a 15sec dissociation step at 92°C and a polymerization step at 60°C for 1min. The changes in Ct values (ΔCt) for the housekeeping gene β-actin were obtained by subtracting the Ct value of the vehicle (DMSO) control cells from the Ct value for the MK886 treated cells. The ΔCt values for the genes of interest were similarly obtained. A normed (ΔΔCt) was calculated for each sample by subtracting the ΔCt value of the housekeeping gene β-actin (ACTB) from the ΔCt value for the gene of interest.

Relative Cellular Protein Levels Measured by Flow Cytometry. Levels of specific proteins in control and MK886-treated LN18 cells were compared via flow cytometry using anti-vinculin (Upstate, Clone V284) and anti-β-actin (Sigma, Clone AC15) primary antibodies and goat anti-mouse-$(Fab)_2$ phycoerythrin-conjugated secondary antibodies (Jackson Laboratories). Cells were collected by trypsinization, washed with PBS, and then fixed with formalin for 15min (Caltag Laboratories Fix & Perm kit). All primary antibodies were diluted to 5ng/μl reaction concentration in Caltag permeabilization buffer and incubated with the fixed LN18 cells for 30min. Anti-Keyhole Limpet Hemocyanin (anti-KLH, Biolegend, Clone MG335) was used as a primary antibody negative control. Following primary antibody incubation, cells were washed by centrifugation (400g for 5min) and incubated for 20 min with appropriate phycoerythrin-conjugated secondary antibodies (1.5ng/μl in PBS, 0.7% BSA). The cells were then washed in PBS and the fluorescence of the vehicle control cells (DMSO) and MK886-treated cells were compared by flow cytometry as described.

Results

MK886 Induces Apoptotic Cell Death in LN18 Cells. The rounding of cells is a classic apoptotic alteration associated with disruption of focal adhesions [20]. The fluorescent micrographs of Fig. 1 illustrate apoptotic morphological changes in LN18 cells following treatment with 50μM MK886. Visualization of actin stress fibers in DMSO vehicle control cells that are adhering to form a monolayer is illustrated in Fig. 1a. with an accompanying punctate staining of vinculin in the cell illustrating focal adhesion points (Fig. 1b). Upon treatment with MK886 for 13h, disorganization of the cytoskeleton and a lack of actin stress fibers accompanied by cellular rounding are illustrated in Fig. 1c along with a diffuse, globular appearance of vinculin (Fig. 1d). Following treatment with MK886 for 18h the complete disorganization of actin (Fig. 1e) and vinculin (Fig. 1f) were manifested along with the formation of apoptotic membranous blebs.

To further demonstrate apoptosis, LN18 cells were treated with indicated concentrations of MK886 for 10h or 15h then assayed for release of DNA-histone complexes from the nucleus into the cytosol. Table 1 shows that by 10-15h MK886, at 30-50μM, induced a significant release of his-

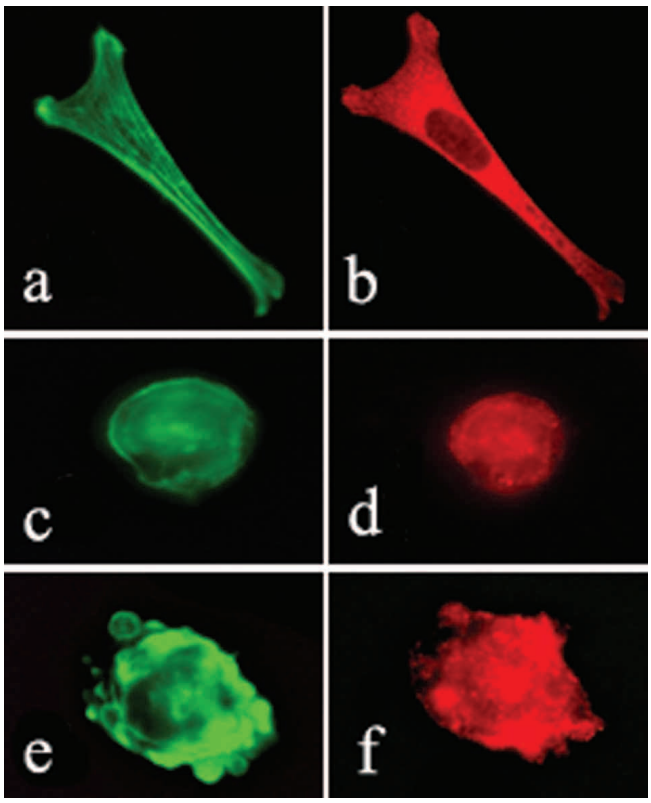

Fig. 1. Fluorescent micrograph (600X) of apoptotic morphological changes in the LN18 glioblastoma induced by MK886. Actin cytoskeleton visualized by phalloidin-488 (a, c, e). Vinculin illustrated by mouse anti-vinculin followed by goat anti-mouse IgG conjugated to Cy3 (b, d, f). Non-treated LN18cells attached and forming actin stress fibers (a) and concentrations of vinculin within focal adhesions on the outer edge of the cell (b). Morphological changes after being treated with 50μM of MK886 for 13h showing rounding (c, d) and apoptotic blebbing by 18h (e, f).

TABLE 1. MK886 Induced Nucleosome Release from LN18 Cells

	MK886 Concentration[1]	$A_{405\ nm}$ [2]
15h	0 (DMSO Control)	0.21 +/-0.07
	5μM	0.22 +/-0.07
	10μM	0.29 +/-0.05
	30μM	1.14 +/-0.20
	50μM	1.57 +/-0.05
	50μM + 50μM ZVAD-FMK	0.31 +/-0.09
10h	0 (DMSO Control)	0.25 +/-0.04
	5μM	0.24 +/-0.04
	10μM	0.24 +/-0.05
	30μM	1.06 +/-0.06
	50μM	1.76 +/-0.11
	50μM + 50μM ZVAD-FMK	0.43 +/-0.07

[1]LN18 cells were treated with indicated concentrations of MK886 for 15h or 10h, as indicated, in the absence or presence of 50μM ZVAD-FMK.
[2]Results show the Absorbance at 405 nm, +/- standard deviation for 8 replicates; higher A_{405} indicate more DNA-histone complexes were released.

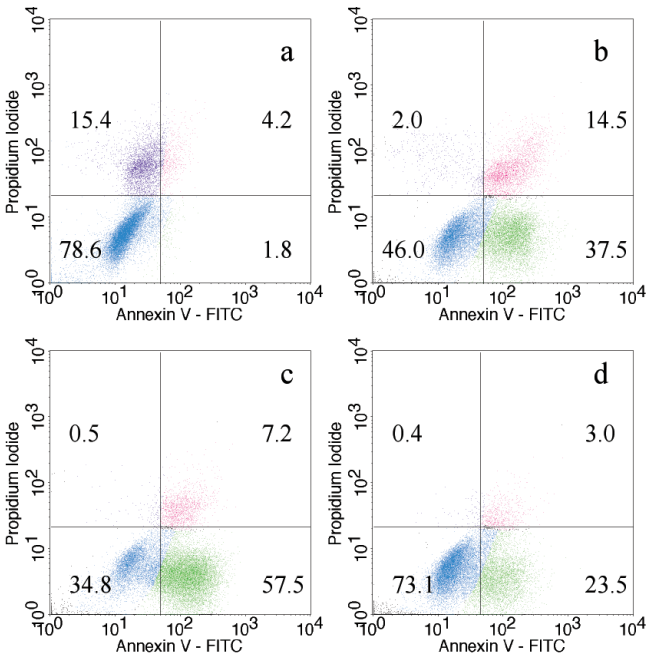

Fig. 2. Induction of apoptosis in LN18 glioblastoma cells. Cells were treated with MK886 at final concentrations of either 30μM (b) or 50μM (c) or in the presence of both 30μM MK886 and 50μM ZVAD-FMK (d) or with the vehicle (DMSO) alone (a). Following 12h incubation cells were harvested, labeled with annexinV and propidium iodide and analyzed by flow cytometry as described in material and methods. Numbers denoted in quadrants of each plot represent the percentage cells positive for annexinV and/or propidium iodide for the total population. Viable cells are represented by the lower left quadrant (blue), necrotic cells are represented by the upper left quadrant (purple), apoptotic in the lower right (green) and late apoptotic or necrotic cells in the upper right quadrant (pink). Data are representative of six experiments.

tone-associated DNA-fragments into the cytosol. Furthermore, the release of DNA fragments was inhibited by the broad caspases inhibitor ZVAD-FMK, indicating that MK886-induced degradation of DNA in LN18 cells is caspases-dependent.

While nucleosome release indicates apoptosis, it is a late marker based on whole culture lysates and does not address single cell phenotypic variations. Therefore LN18 cultures were analyzed for early events in MK886-induced apoptosis on a single cell basis by flow cytometry. LN18 cells were treated with 50μM MK886 for 12h and assessed for annexinV-binding and propidium iodide exclusion by flow cytometry. The upper right and lower right quadrants of Fig. 2a show that in the absence of MK886 few cells are annexinV positive (1.8%) or both annexinV positive and propidium iodide positive (4.2%). At 30μM MK886 (Fig. 2b) and 50μM MK886 (Fig. 2c) a significant percent of LN18 cells entered apoptosis in the absence of necrosis, as indicated by the lower right quadrants showing annexinV-labeled cells devoid of propidium iodide uptake. However, a small population of MK886-treated cells exhibited annexinV-binding accompanied by propidium iodide uptake (upper right quadrants of Figs. 2b and 2c). These cells were either necrotic or in late apoptosis with compromised plasma membranes. AnnexinV-binding is an early event in apoptosis and the caspases inhibitor ZVAD-FMK (50μM) only slightly inhibited the non-necrotic MK886-induced annexinV-binding as shown by the lower right quadrant of Fig. 2d. The ZVAD-FMK more effectively inhibited the necrotic or late apoptotic annexinV-binding demonstrated by the upper right quadrants of Figs. 2b and 2c.

The ability of MK886 to alter the function of mitochondria in LN18 cells was investigated using Mito Tracker Deep Red 633. Cells within an 80% confluent monolayer treated with 30μM or 50μM MK886 (Figs. 3a and 3b respectively) exhibited a marked decrease in Mito Tracker Deep Red 633 fluorescence intensity indicating alteration of mitochondrial oxidative function and possibly a decrease in mitochondrial mass. In addition the data of Fig. 3c show that MK886-induced changes in mitochondrial oxidative function and mass were not inhibited by 50μM of the caspases inhibitor ZVAD-FMK.

The flow cytometry histograms of Fig. 4, showing Mito Tracker Deep Red 633 fluorescence intensity vs. cell count, provide additional evidence that MK886 induced apoptosis in LN18 cells reduced the intensity of Mito Tracker Deep Red 633 fluorescence. Curve "a" is a bimodal histogram showing that the MK886 treated cells within a highly confluent monolayer consist of two populations that are in different states of mitochondrial function indicating that MK886 induced apoptosis is a stochastic process. It also indicates that a long standing (5 days) highly confluent monolayer with stable focal adhesions has a population of cells that are more resistant to apoptosis. This differs from Fig. 3 where the monolayer was 80% confluent and the decrease in Mito Tracker intensity was more homogenous indicating the cells were more uniformly susceptible to apoptosis. Curve "b" of Fig. 4 is a single peak histogram resulting from cells in the monolayer that were gated as annexinV positive and propidium iodide negative thereby consisting of the apoptotic non-necrotic population of cells. It can be seen that the cells of Curve "b" have a lower Mito Tracker Deep Red 633 fluorescence intensity than the cells of Curve "c" obtained by gating on the non-apoptotic population that were annexinV negative and propidium iodide negative.

MK886-Induced Apoptosis is Associated with Down-Regulation of Vinculin. We examined the influence of MK886 on the steady state mRNA expression of β-actin and various focal adhesion proteins by real-time RT-PCR. The data of Fig. 5 show a plot of cycle number vs. normalized fluorescence indicating the results of real time RT-PCR for β-actin. Curve A of Fig. 5 shows the vehicle control and curve B shows MK886 treated cells with 50μM for 15h. It can be seen there is no difference in steady-state mRNA β-

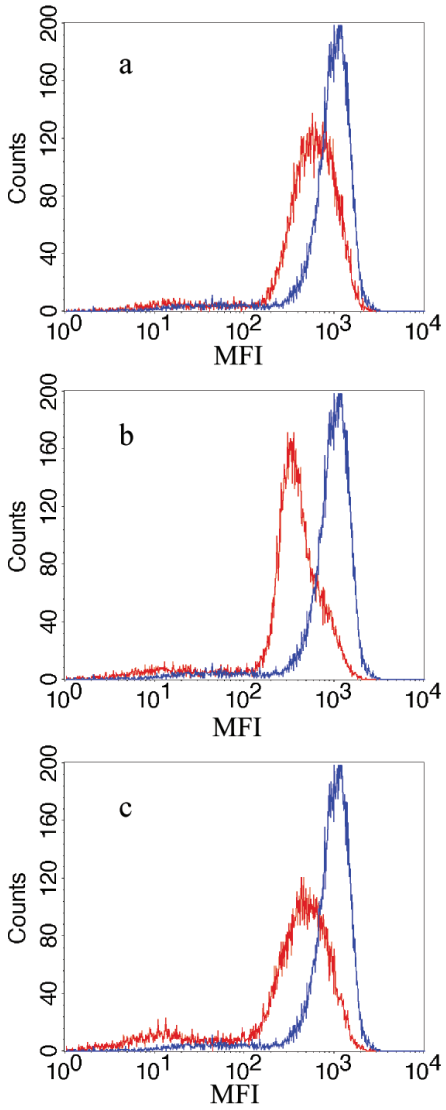

Fig. 3. MK886 treatment induces apoptosis by a mitochondrial pathway. Cells were treated for 10h with either 30μM (a) or 50μM (b) MK886 or with 30μM MK886 and 50μM ZVAD-FMK (c). Cells were harvested and labeled with Mitotracker Deep Red 633 dye and analyzed by flow cytometry as outlined in material and methods. Histograms represent fluorescence intensity of Mito Tracker Deep Red 633 dye where a decrease in fluorescence indicates a decrease in mitochondrial function and mass, indicative of apoptosis. The peak with the higher intensity histogram (blue) represents fluorescence intensity of cells treated with DMSO only and lower intensity histogram (red) represents cells treated with MK866 (a and b) or with both MK866 and ZVAD-FMK (c). Data are representative of six experiments.

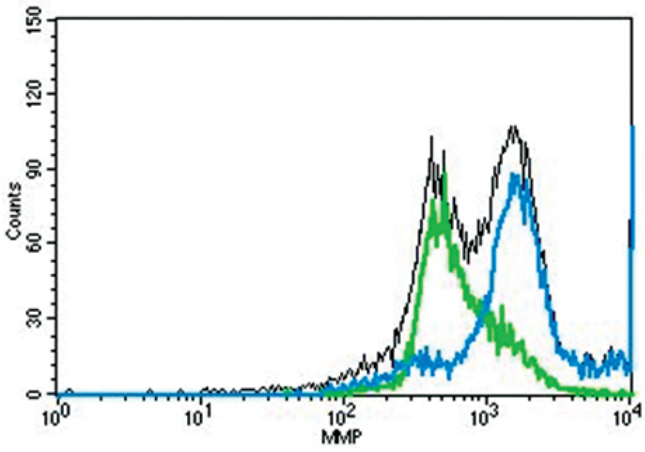

Fig. 4. Composite of flow cytometry histograms showing Mito Tracker Deep Red 633 fluorescence intensity vs. cell count of a population of LN18 cells harvested from a highly confluent monolayer treated with MK886 for 15h. Curve "a" (black) shows the total population of MK886 treated cells as a bimodal histogram of lower and higher fluorescence intensity. Curve "b" (green) illustrates the population of cells of lower fluorescence intensity that were gated as annexinV positive and propidium iodide negative. Curve "c" (blue) illustrates the population of cells of higher fluorescence intensity that were gated as annexinV negative and propidium iodide negative.

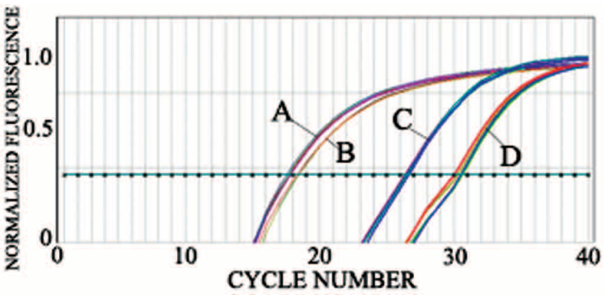

Fig. 5. Measurement of mRNA expression for vinculin and β-actin. Data were accumulated by real time RT-PCR. cDNA(s) were generated from RNA isolated from both MK886 treated and vehicle control LN18 cells. PCR amplicons were generated with primer and probes that were specific for vinculin and β-actin. The abscissa values at the intersections of the horizontal threshold line and the graphs indicate the number of cycles to threshold (Ct). Graphs illustrate the decrease in steady state mRNA expression of vinculin in LN18 cells treated with 50μM MK886 for 15h (D) as compared to DMSO control cells (C). The data show little difference in expression for β-actin in the MK886 treated cells (B) as compared to the DMSO vehicle control cells (A). Data are representative of four experiments.

actin expression when comparing vehicle control cells to MK886 treated cells. Curve C illustrates the vinculin expression in the vehicle control cells while curve D shows the vinculin expression in the MK886 treated cells. The graphs show a down regulation for vinculin in the MK886 treated cells (curve D) as compared to control cells (curve C) while there was little to no change in the expression of β-actin. The data of Table 2 show the effect on mRNA levels of various genes where LN18 cells were exposed to 50μM MK886 for 10h or 15h. A normed (ΔΔCt) was calculated for each sample by subtracting the ΔCt value of β-actin from the ΔCt value for the gene of interest. Vinculin mRNA levels were depressed after 10h and 15h of MK886 treatment, while MK886 elicited little, if any, effects on the mRNA levels of

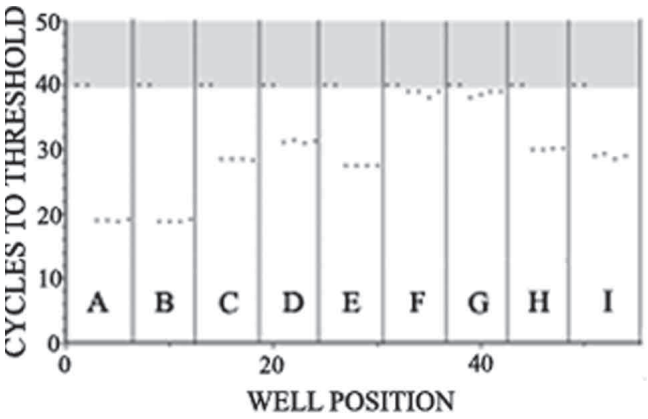

Fig. 6. Measurement of mRNA expression for lipoxygenases and PPAR-α. cDNAs were generated from RNA isolated from untreated LN18 cells. PCR amplicons were generated with primer and probes that were specific for β-actin (A), glyceraldehyde-3-phosphate dehydrogenase (B), E3-lipoxygenase (C), 5-lipoxygenase (D), five lipoxygenase activating protein (E), 12B-lipoxygenase (F), 12P-lipoxygenase (G), 15B-lipoxygenase (H) and peroxisome proliferator activated receptor alpha (I). Cycles to threshold (Ct) were obtained from the fluorescence vs. cycle number curves intersecting with a fixed threshold line where the threshold line was set to intersect at the log phase of the curves (not shown). There are 2 replicate blanks and 4 replicate samples for each gene tested. The total number of cycles to completion of the PCR portion of the experiment was 40. The duplicate blank controls, for which reverse transcriptase was omitted, are presented as having Ct values of 40 because the samples did not reach threshold within 40 cycles. The displayed Ct values for the 4 replicates of each sample indicate the level of mRNA in the untreated LN18 cells. Sample Ct values being significantly less than 40 indicate there was a steady state mRNA expression. There was little to no expression of the 12-lipoxygenases.

the other genes examined that play a role in the formation and stabilization of focal adhesions.

PPAR-α and FLAP are Expressed in LN18 cells. Real time RT-PCR was used to determine if the steady state mRNAs for FLAP and PPAR-α, as well as other select genes involved in metabolizing arachidonate, were expressed in LN18 cells. Fig. 6 is a plot of the number of cycles to threshold versus the sample well position for untreated LN18 cells. There are two blank replicates (greater than 40 cycles to threshold) and four sample replicates for each gene measured. The data show relatively low Ct values for the housekeeping genes β-actin (A) and glyceraldehyde-3-phosphate dehydrogenase (B), indicating high expression of mRNA for these genes. Fig. 6 also demonstrates that mRNAs for both PPAR-α (I) and FLAP (E) are readily detected in LN18 cells. Furthermore, while mRNAs for ALOX-E3 (C), ALOX-5 (D) and ALOX-15B (H) were expressed, little if any, mRNAs coding ALOX-12B (F) or ALOX-12P (G) were detected in LN18 cells.

To determine if the MK886-mediated reduction of vinculin mRNA (Fig. 5 & Table 2) resulted in a corresponding drop in vinculin protein, cells were analyzed by flow cytometry for intracellular levels of vinculin, as well as for β-actin. The flow cytometry histograms of Fig. 7 compare MK886 treated cells to non-treated vehicle control cells (DMSO) for both vinculin and β-actin. The vinculin histograms of Fig. 7 show that vinculin levels are reduced by treating LN18 cells with 50μM MK886 for 16h as demonstrated by the 3 fold drop in the mean fluorescence intensity. The data of Fig. 7 show also that the protein levels of b-actin are minimally impacted in LN18 cells by similar treatment with MK886.

TABLE 2. Effect of MK886 on the level of specific mRNAs in LN18 cells[1,2]

GENE DESIGNATION	Ct CONTROL 10h	Ct MK886 10h	ΔΔCt MK886 10h	ΔΔCt MK886 15h
β- ACTIN (ACTB)	17	18	NA	NA
VINCULIN (VCL)	26	31	4	3
FOCAL ADHESION KINASE (FAK)	24	24	-1	0
PAXILLIN (PXN)	26	27	0	0
TALIN-2 (TLN2)	27	27	-1	1
CATENIN (CTNNA1)	19	19	-1	ND
INTEGRIN-α 5 (ITGA5)	19	20	0	1
INTEGRIN-α V (ITGAV)	19	20	0	-1
INTEGRIN-β 1 (ITGB1)	19	20	0	0
INTEGRIN- β 3 (ITGB3)	23	24	0	0
INTEGRIN- β 5 (ITGB5)	20	21	0	1
CADHERIN2 (CDH2)	20	21	0	ND
RHO GTPASE ACTIVATING PROTEIN-26 (ARHFGAP26)	22	23	0	ND

[1]Real time RT-PCR was used to determine the Ct values for the specific mRNAs (Genes) indicated in untreated (Control) LN18 cells and cells exposed to 50μM MK886 for 10h or 15h.

[2]The changes in Ct values (ΔCt) for each mRNA were obtained by subtracting the Ct value of the DMSO control cells from the Ct value for the MK886 treated cells at 10h. The Ct values for β-actin did not change significantly for the MK886 treated cells as compared to control cells. A normed (ΔΔCt) was calculated for each sample by subtracting the ΔCt value of β-actin from the ΔCt value for the gene of interest. The Ct values for the calculation of the 10h ΔΔCt values (column 4) are shown above, but the Ct values for the calculation of the 15h ΔΔCt values (column 5) are not shown.

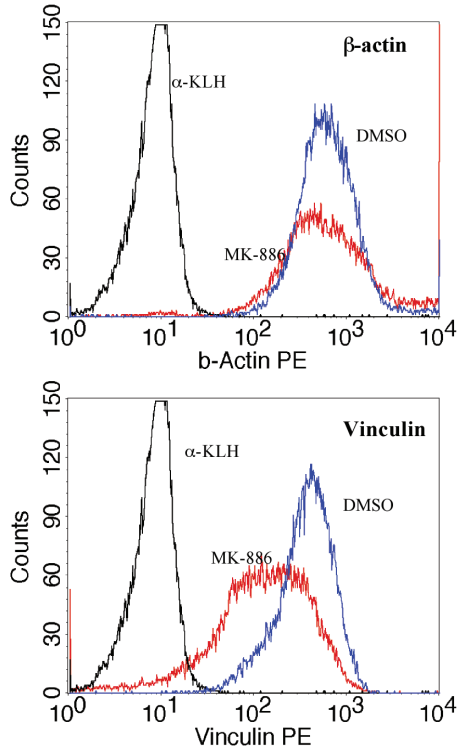

Fig. 7. MK886 treatment reduces protein levels of vinculin in LN18 cells. Formalin fixed cells were treated with antibody specific for β-actin or vinculin followed by anti-mouse-F(ab)$_2$ conjugated to phycoerythrin and subsequently analyzed by flow cytometry as described in material and methods. In the graphs of the figure the blue histogram indicates the non-treated vehicle control (DMSO) and the red histogram indicates the results for 50μM MK886 treated cells for 16h. The β-actin histograms show no change in intensity for MK886 treated cells as compared to controls. A clear down shift in the intensity of the vinculin histograms can be seen for the MK886 treated cells (red) as compared to the DMSO control (blue). Non-specific labeling was monitored using anti-KLH control antibody (grey scale histograms of lowest intensity). Data are representative of three experiments.

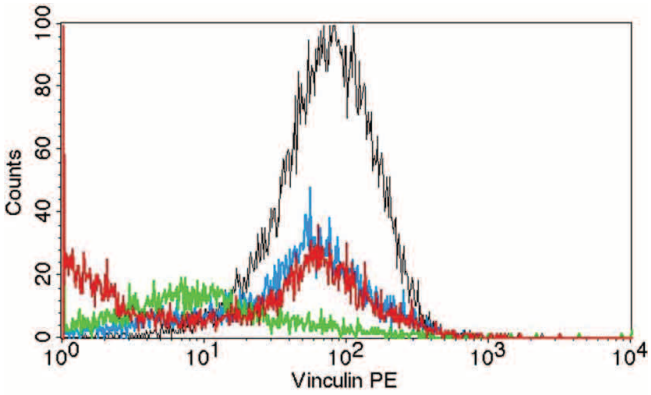

Fig. 8. Decreased vinculin is associated with the apoptotic non-necrotic population of cells. The curve (black) is a single histogram of all of the vehicle control cells that expressed vinculin. The MK886 treated cells (15h) are represented by three histograms (blue, red, and green) which resulted from gating on the annexinV negative and 7-AAD negative (blue) or annexinV negative and 7-AAD positive (red) or annexinV positive and 7-AAD negative (green). It can be seen that the apoptotic population (green) shows a marked decrease in vinculin as manifested by a lower fluorescence intensity compared to the control cells (black).

The histograms of Fig. 8 show that the decrease in vinculin is associated with the apoptotic population of LN18 cells. The histogram of the vehicle control cells (black) show the fluorescent intensity indicating the level of vinculin of the total population of the control cells. The MK886 treated cells (15h) were gated into three populations which include annexinV negative and 7-AAD negative (blue), annexinV negative and 7-AAD positive (red), and annexinV positive and 7-AAD negative (green). The non-necrotic apoptotic cells (green) were the only population that showed a down-regulation of vinculin protein as compared to the control cells (black).

Discussion

As previously mentioned, one approach to improve cure rates of treatment refractory glioblastomas is to target multiple apoptotic pathways with an understanding of the cell signaling and apoptotic mechanisms involved [21]. MK886 is an anti-tumor drug that induces apoptosis in various types of cancer cells most likely by targeting multiple pathways [4, 5, 7, 13, 18]. However, a full understanding of the mechanism of MK886-induced apoptosis has not yet been established. The LN18 glioblastoma cell line was chosen for this study because it exhibits genetic characteristics useful for apoptotic studies, including mutated p53 with a wild-type PTEN gene [22] and a functional Fas receptor [23]. In addition, the efficacy of MK886 in inducing apoptosis in glioblastoma cells had not been studied. In this present paper, MK886-induced apoptosis in LN18 cells was manifested by release of nuclear DNA-histone complexes, annexinV-binding, and altered mitochondrial function. The involvement of a mitochondrial pathway in MK886-induced apoptosis in LN18 cells is consistent with the pathway of MK886-induced apoptosis in prostate cancer cells [24]. Furthermore, the broad caspases inhibitor, ZVAD-FMK, effectively inhibited MK886-induced nucleosome release, but was less effective in preventing annexinV-binding or altered mitochondrial oxidative function and mass, indicating that the apoptotic phosphatidylserine exposure and changes in mitochondrial function are caspases independent. This is in agreement with the report by Lugli et al. [25] stating that a decrease in mitochondrial mass is an early event in apoptosis that precedes permeability to propidium iodide and DNA condensation and fragmentation.

Whether FLAP and PPAR-α, as proteins that MK886 can impact, are expressed in LN18 glioblastoma cells had not been determined. Real time RT-PCR demonstrated that mRNAs for FLAP and PPAR-α are readily detected in LN18 cells. The biosynthesis of leukotrienes can exert varied biological ac-

tivities, including leukotriene-B_4 activation of the transcription factor PPAR-α [15]. Numerous studies have also implicated lipoxygenase metabolites in the proliferation and survival of a variety of tumors [26–29]. Therefore, pharmacological intervention of leukotriene metabolism represents a potential strategy for investigating the treatment of certain types of cancers including glioblastomas.

PPAR-α is a member of the nuclear hormone receptor superfamily which contains transcription factors involved in varied and diverse processes, including apoptosis [30]. Activated PPAR-α can suppress apoptosis [31] while inhibition of PPAR-α has been shown to induce apoptotic cell death in a variety of cell types, thereby increasing enthusiasm for the potential of PPAR-α inhibition as a chemotherapeutic strategy [32, 33]. Over the past several years interest has developed in the use of lipoxygenase inhibitors in combination with PPAR-α inhibitors as chemotherapeutic agents for the treatment of malignant tumors [34].

At 10-15h MK886 had little, if any, effect on the level of β-actin mRNA in LN18 cells. This is in contrast to a recent study indicating that in serum free medium MK886 altered actin expression in a number of cell lines [35]. The conflicting results on the degree to which MK886 alters actin expression may be due to differences in concentrations of MK886, length of time of MK886 exposure, the degree of necrosis vs. apoptosis, concentrations of serum in culture media during exposure, and/or the different cell lines used in the different studies. Furthermore, Mayburd et al. [35] did not detect significant MK886-dependent changes in vinculin expression in cell lines used in their studies. However, the data presented here clearly indicate that treatment of LN18 cells with 50μM MK886 down-regulates vinculin protein levels while no decreases in β-actin expression were detected.

Following treatment with MK886, LN18 cells change in morphology and round up indicating a disruption of focal adhesion attachments. The drop in expression and levels of the focal adhesion protein vinculin could be one aspect of the mechanisms by which cells treated with MK886 change in fluidity and morphology. Vinculin is associated with a large number of cytoskeletal and focal adhesion proteins including talin [36], actinin [37], actin [38] and paxillin [39]. These multiprotein complexes are further associated with cell adhesion signaling molecules important to rendering cells susceptible or resistant to apoptosis [40]. As aforementioned, our data show that MK886 induction of apoptosis in LN18 cells is associated with decreased vinculin protein levels. However, other studies indicate that cells having poor organization of vinculin are metastatic [41], while cells lacking vinculin, such as $vin^{-/-}$ F9 mouse embryonal carcinoma cells manifest enhanced survival [42, 43] and high motility [44]. The increased survival of $vin^{-/-}$ cells is proposed to be due to up-regulated activity of extracellular signal–regulated kinase (ERK) which results from vinculin's modulation of paxillin–FAK interactions [43]. However, the study by Subauste et al. [43] is not in total agreement with the study of Howe et al. [42] which reports an up-regulated ERK activity when cells are in contact with an extra cellular matrix and being integrin stimulated with stable focal adhesions. Reports that focus on the structure of vinculin reveal the importance of the intramolecular interaction between the head and tail domains of vinculin which regulates the conformations of vinculin that result in auto-inhibition or activation [45]. Chen et al. [46] showed that activated vinculin is concentrated at the proximal edge of gliding focal adhesions whereas only a fraction of vinculin was found in the activated state in stable protruding adhesions which could be an explanation for the differences between the data of Howe et al. [42] and Subauste et al. [43]. Thus, the role of vinculin in cellular processes is complicated and additional studies are needed to determine the reasons why some vinculin-deficient cells appear apoptosis-resistant, while in the LN18 cells MK886-induced apoptosis is accompanied by a reduction in vinculin protein levels.

When tissue cells round up and are removed from an extracellular matrix they become susceptible to self-destruction, even in the presence of sufficient growth factors [47]. The process of enhanced programmed cell death in cells free from a matrix has been coined anoikis [48]. When cancer cells metastasize they escape anoikis and subsequently become fixed in a matrix away from the primary site whereupon the extracellular matrix renders the cells more resistant to chemotherapeutic agents. Cells in contact with an extracellular matrix are known to manifest an increased resistance to apoptosis. A proposed mechanism for this is that focal adhesions rescue cells from apoptosis through transduction proteins and the scaffolding of an array of kinases that initiate an anti-apoptotic cascade resulting in the phosphorylation and inactivation of the pro-apoptotic proteins Bad and caspase-9 [49, 50]. The data presented here indicate that the down-regulation of vinculin is associated with MK886 induced apoptosis and the rounding up of apoptotic cells. Rounded up cells more loosely attached to a matrix with disrupted focal adhesions could be rendered more susceptible to anoikis, and also more susceptible to *in vivo* phagocytosis and immunological defense mechanisms that come in to play in the elimination of aberrant cells. The rapid activation of phagocytic microglial cells accompanies most CNS pathologies [51–53]. The possibility that apoptotic glioblastoma cells that have rounded up, in a state of down-regulated vinculin, expose determinants that activate microglial cells has not escaped our interest.

Although *in vitro* apoptotic studies on cultured tumor cells do not necessarily accurately predict clinical effectiveness, such studies can substantially increase an understanding of apoptotic cell signaling mechanisms. We conclude that MK886 effectively induces apoptosis in the LN18 cells concomitant with down-regulation of vinculin protein. Elucidating the mechanism of MK886-induced apoptosis in these cells, along with further investigation of the anti-apoptotic role of integrin stimulation and focal adhesions in the context of apoptosis, offers a potential chemotherapeutic strategy in the treatment refractory glioblastomas.

This work was supported in part by funding provided by West Virginia EPSCoR Grant EPS2006-15 and NIH Grant Number 1P20RR16477 from the National Center for Research Resources.

References

[1] YUNG WK, ALBRIGHT RE, OLSON J, et al. A phase II study of temozolomide vs. procarbazine in patients with glioblastoma multiforme at first relapse. Br J Cancer 2000; 83: 588–593.

[2] STUPP R, MASON WP, van den BENT MJ, et al. The European Organisation for Research and Treatment of Cancer Brain Tumor and Radiotherapy Groups and the National Cancer Institute of Canada Clinical Trials Group Radiotherapy plus Concomitant and Adjuvant Temozolomide for Glioblastoma. New England J of Med 2005; 352:987–996. (Clinical Study, Abstract)

[3] HEGI ME, DISERENS AC, GORLIA T, et al. MGMT gene silencing and benefit from temozolomide in glioblastoma. New England J Med 2005; 352: 997–1003.

[4] DIXON RAF, DIEHL RE, OPAS E, et al. Requirement of a 5-lipoxygenase- activating protein for leukotriene synthesis. Nature 1990; 343: 282–284.

[5] MILLER DK, GILLARD JW, VICKERS PJ, et al. Identification and isolation of a membrane protein necessary for leukotriene production. Nature 1990; 343: 278–281.

[6] FORD-HUTCHINSON AW. FLAP: A novel drug target for inhibiting the synthesis of leukotrienes. Trends Pharmacol Sci 1991; 12: 68–70.

[7] ANDERSON KM, SEED T, JAJEH A, et al. An in vivo inhibitor of 5-lipoxygenase, MK886, at micormolar concentration induces apoptosis in U937 and CML cells. Anticancer Res 1996; 16(5A): 2589–2599.

[8] GHOSH J and MYERS CE. Inhibition of arachidonate 5-lipoxygenase triggers massive apoptosis in human prostate cancer cells. Proc Natl Acad Sci USA 1998; 95: 13182–13187.

[9] GHOSH J and MYERS CE. Arachidonic acid stimulates prostate cancer cell growth: Critical role of 5-lipoxygenase. Biochem Biophys Res Commun 1997; 235(2): 418–423(6).

[10] TONG WG, DING XZ, ADRIAN TE. The mechanisms of lipoxygenase inhibitor- induced apoptosis in human breast cancer cells. Biochem Biophys Res Commun 2002; 296: 942–948.

[11] DING XZ, TONG WG, ADRIAN TE. Cyclooxygenases and lipoxygenase potential targets for treatment of pancreatic cancer. Pancreatology 2001; 1: 91–99.

[12] ROMANO M AND CLARIA J. Cyclooxygense-2 and 5-lipoxygenase converging function on cell proliferation and tumor angiogenesis: implications for cancer therapy. FASEB J 2003; 17: 1986–1995.

[13] DATTA K, BISWAL SS, KEHRER JP. The 5-lipoxygenase-activating protein (FLAP) inhibitor, MK886, induces apoptosis independently of FLAP. Biochem J 1999; 340: 371–375.

[14] YU K, BAYANO W, KALLEN CB, et al. Diverential activation of peroxisome proliferator-activated receptors by eicosanoids. J Biol Chem 1995; 270: 23975–23983.

[15] DEVCHAND PR, KELLER H, PETERS JM, et al. The PPARα-leukotriene B4 pathway to inflammation control. Nature 1996; 384: 39–43.

[16] FORMAN BM, CHEN J, EVANS RM. Hypolipidemic drugs, polyunsaturated fatty acids, and eicosanoids are ligands for peroxisome proliferator-activated receptors alpha and delta. Proc Natl Acad Sci USA 1997; 94: 4318–4323.

[17] KLIEWER SA, SUNDSETH SS, JONES SA, et al. Fatty acids and eicosanoids regulate gene expression through direct interactions with peroxisome proliferator-activated receptors α and δ. Proc Natl Acad Sci USA 1997; 94: 4312–4317.

[18] KEHRER JP, BISWAL SS, THUILLIER P, et al. Inhibition of peroxisome proliferator- activated receptor alpha (PPARα) by MK886. Biochem J 2001; 356: 899–906.

[19] DISERENS AC, DE TRIBOLET N, MARTIN-ACHARD A, et al. Characterization of an established human malignant glioma cell line: LN-18. Acta Neuorpathol 1981; 53: 21–28.

[20] HACKER G. The morphology of apoptosis. Cell Tissue Res 2000; 301: 5–17.

[21] McCARTY MF. Targeting multiple signaling pathways as a strategy for managing prostate cancer: multifocal signal modulation therapy. Integrative Cancer Therapies 2004; 3: 349–380.

[22] ISHII N, MAIER D, MERLO A, et al. Frequent co-alterations of TP53, p16/CDKN2A, p14ARF, PTEN tumor suppressor genes in human glioma cell lines. Brain Pathol 1999; 9: 469–479.

[23] SCHLAPBACH R AND FONTANA A. Differential activity of bcl-2 and ICE enzyme family protease inhibitors on FAS and puromycin-induced apoptosis of glioma cells. Biochim Biophys Acta 1997; 1359: 174–180.

[24] GUGLIUCCI A, RANZATO L, SCORRANO L, et al. Mitochondria are direct targets of the lipoxygenase inhibitor MK886. A strategy for cell killing by combined treatment with MK886 and cyclooxyenase inhibitors. J Biol Chem 2002; 277(35): 31789–31795.

[25] LUGLI E, TROIANO L, FERRARESI R, et al. Characterization of cells with different mitochondrial membrane potential during apoptosis. Cytometry Part A 2005; 28–35.

[26] DIN XZ, KUSZYNSKI CA, EL-METWALLY TH, et al. Lipoxygenase inhibition induced apoptosis, morphological changes, and carbonic anhydrase expression in human pancreatic cancer cells. Biochem Biophys Res Commun 1999; 392–399.

[27] GHOSH J and MYERS CE. Central role of arachidonate 5-lipoxygenase in the regulation of cell growth and apoptosis in human prostate cancer cells. Adv Exp Med Biol 1999; 469: 577–582.

[28] STEELE VE, HOLMES CA, HAWK ET, et al. Lipoxygenase inhibitors as potential cancer chemopreventives. Canc Epidemiol Biomarkers Prev 1999; 8: 467–483.

[29] SHUREIQI I AND LIPPMAN SM. Lipoxygenase modulation to reverse carcinogensis. Cancer Res 2001; 61: 6307–6312.

[30] LEMBERGER T, DESVERGNE B, WAHLI W. PPARs: a nuclear receptor signaling pathway in lipid metabolism. Annu Rev Cell Dev Biol 1996; 12: 335–363.

[31] ROBERTS RA, JAMES NH, WODDYATT NJ, et al. Evidence for the suppression of apoptosis by the peroxisome proliferator

activated receptor alpha (PPARα). Carcinogensis 1998; 19: 43–48.
[32] MICHALIK L, DESVERGNE B, WAHLI W. Peroxisome-proliferator-activated receptors and cancers: complex stories. Nat Rev Cancer 2004; 4: 61–70.
[33] NAAGOTHU KK, BHATT R, KAUSHAL GP, PORTILLA D. Fibrate prevents cisplatin-induced proximal tubule cell death. Kidney Int 2005; 68(6): 2680–2693.
[34] MULSHINE JL and JETT M. Use of lipoxygenase inhibitors and PPAR ligands as anti-cancer therapeutic and intervention agents. US Patent 2004; #6, 756, 399.
[35] MAYBURD AL, MARTINEZ A, SACKETT D, et al. Ingenuity network-assisted transcription profiling: Identification of a new pharmacologic mechanism for MK886. Clinic Canc Res 2006; 12(6): 1820–1827.
[36] BURRIDGE K and MANGEAT P. An interaction between vinculin and talin. Nature 1984; 308: 744–746.
[37] BELKIN AM and KOTELIANSKY VE. Interaction of iodinated vinculin, metavinculin, and alpha-actinin with cytoskeletal protein. FEBS Lett 1987; 220: 291–294.
[38] RUHNAU K and WEGNER A. Evidence for direct binding of vinculin to actin filaments. FEBS 1988; 228: 105–108.
[39] TURNER CE, GLENNEY JR Jr., BURRIDGE K. Paxillin: a new vinculin-binding protein present in focal adhesions. J Cell Biol 1990; 111: 1059–1068.
[40] RUOSLAHTI E AND OBRINK B. Common principles in cell adhesion. Exp Cell Res 1996; 227: 1–11.
[41] RAZ A and GEIGER B. Altered organization of cell-substrate contacts and membrane-associated cytoskeleton in tumor cell variants exhibiting different metastatic capabilities. Cancer Res 1982; 42: 5183–5190.
[42] HOWE AK, ALPIN AE, JULIANO RL. Anchorage-dependent ERK signaling mechanisms and consequences. Curr Opin Genet Dev 2002; 12: 30–35.
[43] SUBAUSTE MC, PERTZ O, ADAMSON ED, et al. Vinculin modulation of paxillin-FAK interactions regulates ERK to control survival and motility. J Cell Biol 2004; 165(3): 371–381.
[44] COLL JL, BEN-ZE'EV A, EZZELL RM, et al. Targeted disruption of vinculin gene in F9 and ES cells changes cell morphology, adhesion, and locomotion. Proc Nat Acad Sci USA 1995; 92: 9161–9165.
[45] ZIEGLER WH, LIDDINGTON RC, CRITCHLEY DR. The structure and regulation of vinculin. Trends in Cell Biol 2006; 16: 453–460.
[46] CHEN H, COHEN DM, CHOUDHURY DM, et al. Spatial distribution and functional significance of activated vinculin in living cells. J Cell Biol 2005; 169: 459–470.
[47] FRISCH SM AND FRANCIS H. Disruption of epithelial cell-matrix interactions induces apoptosis. J Cell Biol 1994; 124: 619–626.
[48] FRISCH SM and RUOSLAHTI E. Integrins and anoikis. Curr Opin Cell Biol 1997; 9: 701–706.
[49] FRISCH SM, VUORI K, RUOSLAHTI E, CHAN-HUI PY. Control of adhesion-dependent cell survival by focal adhesion kinase. J Cell Biol 1996; 134: 793–799.
[50] DOWNWARD J. Mechanisms and consequences of activation of protein kinase B/Akt. Curr Opin Cell Biol 1998' 10: 262–267.
[51] GIULIAN D, CORPUZ M, CHAPMAN S, et al. Reactive mononuclear phagocytes release neurotoxins after ischemic and traumatic injury to the central nervous system. J Neurosci Res 1993; 36: 681–693.
[52] McGREER PL, KAWAMATA T, WALKER DG, et al. Microglia in degenerative neurological disease. Glia 1993; 7: 84–92.
[53] KREUTZBERG GW. Microglia, the first line of defense in brain pathologies. Arzneimittelforschung 1995; 45: 357–360.